

CHEM MED CHEM

CHEMISTRY ENABLING DRUG DISCOVERY

Accepted Article

Title: Chemoproteomics-aided medicinal chemistry for the discovery of EPHA2 inhibitors

Authors: Stephanie Heinzlmeir, Jonas Lohse, Tobias Treiber, Denis Kudlinzki, Verena Linhard, Santosh Lakshmi Gande, Sridhar Sreeramulu, Krishna Saxena, Xiaofeng Liu, Mathias Wilhelm, Harald Schwalbe, Bernhard Kuster, and Guillaume Médard

This manuscript has been accepted after peer review and appears as an Accepted Article online prior to editing, proofing, and formal publication of the final Version of Record (VoR). This work is currently citable by using the Digital Object Identifier (DOI) given below. The VoR will be published online in Early View as soon as possible and may be different to this Accepted Article as a result of editing. Readers should obtain the VoR from the journal website shown below when it is published to ensure accuracy of information. The authors are responsible for the content of this Accepted Article.

To be cited as: *ChemMedChem* 10.1002/cmdc.201700217

Link to VoR: <http://dx.doi.org/10.1002/cmdc.201700217>

WILEY-VCH

www.chemmedchem.org

A Journal of



Chemoproteomics-aided medicinal chemistry for the discovery of EPHA2 inhibitors

Stephanie Heinzlmeir^{[a],[d],[e],[f]}, Jonas Lohse^[a], Tobias Treiber^[a], Dr. Denis Kudlinzki^{[b],[d],[e]}, Verena Linhard^[b], Dr. Santosh Lakshmi Gande^{[b],[d],[e]}, Dr. Sridhar Sreeramulu^[b], Dr. Krishna Saxena^[b], Dr. Xiaofeng Liu^[c], Dr. Mathias Wilhelm^[a], Prof. Dr. Harald Schwalbe^{[b],[d],[e],*}, Prof. Dr. Bernhard Kuster^{[a],[d],[e],[f],[g],*}, Dr. Guillaume Médard^{[a],*}

- [a] S. Heinzlmeir, J. Lohse, T. Treiber, Dr. M. Wilhelm, Prof. Dr. B. Kuster, Dr. G. Médard
Chair of Proteomics and Bioanalytics
Technical University of Munich
Emil-Erlenmeyer-Forum 5 , 85354 Freising, Germany
g.medard@tum.de, kuster@tum.de
- [b] Dr. D. Kudlinzki, V. Linhard, Dr. S. L. Gande, Dr. S. Sreeramulu, Dr. K. Saxena, Prof. Dr. H. Schwalbe
Center for Biomolecular Magnetic Resonance
Johann Wolfgang Goethe-University
Max-von-Laue-Str. 7, 60438 Frankfurt am Main, Germany
schwalbe@nmr.uni-frankfurt.de
- [c] Dr. X. Liu
Shanghai Key Laboratory of New Drug Design, School of Pharmacy, East China University of Science and Technology, Shanghai, China
- [d] S. Heinzlmeir, Dr. D. Kudlinzki, Dr. S. L. Gande, Prof. Dr. H. Schwalbe, Prof. Dr. B. Kuster
German Cancer Consortium (DKTK), Heidelberg, Germany
- [e] S. Heinzlmeir, Dr. D. Kudlinzki, Dr. S. L. Gande, Prof. Dr. H. Schwalbe, Prof. Dr. B. Kuster
German Cancer Research Center (DKFZ), Heidelberg, Germany
- [f] S. Heinzlmeir, Prof. Dr. B. Kuster
Bavarian Center for Biomolecular Mass Spectrometry (BayBioMS), Technical University of Munich, Freising, Germany
- [g] Prof. Dr. B. Kuster
Center for Integrated Protein Science Munich (CIPSM), Freising, Germany

Abstract

The receptor tyrosine kinase EPHA2 has gained interest as therapeutic drug target in cancer and infectious diseases. However, EPHA2 research and EPHA2-based therapies have been hampered by the lack of selective small molecule inhibitors. Here, we report on the synthesis and evaluation of dedicated EPHA2 inhibitors based on the clinical BCR-ABL/SRC inhibitor Dasatinib as a lead structure. We designed hybrid structures of Dasatinib and the previously known EPHA2 binders CHEMBL249097, PD-173955 and a known EPHB4 inhibitor in order to exploit both the ATP pocket entrance as well as the ribose pocket as binding epitopes in the kinase EPHA2. Medicinal chemistry and inhibitor design was guided by a chemical proteomic approach allowing for early selectivity profiling of the newly synthesized inhibitor candidates. Concomitant protein crystallography of 17 inhibitor co-crystals delivered detailed insight into the atomic interactions that underlie the structure-affinity-relationship. Finally, the anti-proliferative effect of the inhibitor candidates was confirmed in the glioblastoma cell line SF-268. In this work, we thus discovered a novel EPHA2 inhibitor candidate 4a featuring an improved selectivity profile while maintaining potency against EPHA2 and anti-cancer activity in SF-268 cells.

Accepted Manuscript

Introduction

The receptor tyrosine kinase EPHA2 has found increasing interest as a therapeutic target over the past ten years.^[1] In 1994, EPHA2 was linked to carcinogenesis for the first time^[2], and, since, has been implicated in a variety of different pathologies including cancer, infectious diseases and cataract formation.^[1, 3] In oncology, EPHA2 overexpression has been discovered in a wide variety of different cancer entities (e.g. head and neck^[4], prostate^[5], breast^[6], and non-small cell lung cancer^[7]) and is a known driver for carcinogenesis, metastasis, angiogenesis and resistance^[8] of tumors^[1] – ultimately leading to a poor prognosis for affected patients.^[7, 9] In infectious diseases, EPHA2 mediates target cell binding and cell entry via endocytosis of pathogens, such as viruses (KHSV^[10] and Hepatitis C virus^[11]), bacteria (*C. trachomatis*^[12] and *M. tuberculosis*^[13]) or even single cell parasites (*P. falciparum*^[14]). Inhibition of EPHA2 catalytic activity has proven to be beneficial in both disease areas.^[15, 16]

Several therapeutic strategies have been developed to interfere with EPHA2 signaling. These include agonists or antagonists targeting the extracellular ligand binding site and driving endocytosis of the receptor, or inhibition of the intracellular kinase domain by small molecule kinase inhibitors.^[15, 17]

Despite the rising relevance of EPHA2 as a therapeutic drug target, medicinal chemistry efforts aiming at the development of dedicated EPHA2 small molecule inhibitors are still in their infancy.^[18] Owing to this shortage of dedicated chemical inhibitors, the dual BCR-ABL/SRC inhibitor Dasatinib – which also potently targets EPHA2 – has been employed as a surrogate to investigate EPHA2 function and to abrogate EPHA2 signaling in cells.^[19] In fact, Dasatinib is the only drug which is already administered to patients in a number of clinical trials in order to assess the clinical value of EPHA2 inhibition in treating cancer (clinicaltrials.gov). Recently, we reported on 24 known clinical kinase inhibitors that bind EPHA2 as an unintended off-target which substantially expanded the landscape of known EPHA2 inhibitors.^[20] This collection of compounds should enable research to select more appropriate EPHA2 targeting compounds and foster drug repurposing of clinically evaluated molecules for application in EPHA2-dependent diseases. We found Dasatinib to be the most potent known EPHA2 inhibitor but its very promiscuous target profile renders unambiguous interpretation of cell biological and clinical data difficult.

Here we report on a medicinal chemistry effort to develop EPHA2-inhibitors with improved target profiles. We systematically employed chemical proteomics^[21, 22] alongside the medicinal chemistry campaign to profile the potency and selectivity of each and every synthesized molecule in lysates of cancer cells. We hypothesized that this new methodology, which can be described as

“chemoproteomics-aided drug discovery”, could facilitate lead selection and lead optimization by establishing, in a timely manner, the affinity of the molecules for around 250 native kinases and many other ATP-binding proteins as well as potentially toxic off-targets.^[23] This synchronous approach indeed provided valuable guidance during the drug-discovery process and protein crystallography added detailed molecular insight into drug-protein interactions and structure-affinity-relationships at the atomic level. We further demonstrate that the priority compounds discovered in this way show cellular activity against the glioblastoma cell line SF-268 and displayed a favorable selectivity profile over other EPHA2 inhibitors, notably Dasatinib.

Results and Discussion

Hybridization of known EPH receptor binders yields new EPHA2 inhibitor designs

Dasatinib features a very broad target profile with low nanomolar affinities mainly towards tyrosine kinases (TK) such as the ABL family, SRC family or EPH family (Figure 1a). In total, Dasatinib targets 44 protein kinases with sub-micromolar affinity, including many proteins of the TKL, AGC, CAMK subclasses of kinases. We hypothesized that a judicious choice of substituents could improve selectivity while maintaining potency against EPHA2. We therefore first sought to gain a detailed understanding of the molecular interactions governing the binding of Dasatinib to EPHA2. We identified a minimal pharmacophore as a scaffold on which to append relevant chemical moieties found in other EPH receptor binders. Our previously reported crystal structure that determined the binding mode of Dasatinib to EPHA2 (PDB: 5I9Y) established that the pyrimidine moiety of Dasatinib is not engaged in EPHA2 binding. By docking experiments, we discovered that two other known EPHA2 inhibitors, CHEMBL249097^[24] and PD-173955^[20, 25] (Figure 1b), position a phenyl moiety in lieu of the pyrimidine (Supplementary Figure 1). We therefore excluded hetero substitutions from this aromatic ring in our design. The X-ray structure further highlighted two sites amenable for chemical modification – the ribose pocket and the ATP pocket entrance which can both accommodate spatially demanding groups (schematic representation in Figure 1c). On the basis of this analysis, we designed a hybrid structure of Dasatinib and previously described EPHB4 inhibitors^[26] (Figure 1b) to investigate the size of both pockets by introduction of bulky morpholino and methylsulfonyl substituents. In contrast to the ribose pocket, the pocket entrance is rich in selectivity residues, which are defined as side chain exposed and chemically targetable residues with low conservation across the kinome (notably Lys702, Glu706 and Lys617).^[20] Direct interactions of a compound with these charged residues could potentially drive selectivity towards EPHA2 and away from many other kinases. Accordingly, we introduced chemical moieties such as primary and secondary amines, hydroxyl groups or carboxylic acid groups into the molecules. Docking of CHEMBL249097 also revealed a putative interaction between its amide and the backbone of Glu696 located in the hinge region. Since this residue was not engaged by Dasatinib, we probed this interaction by including an amide bond at the *meta*-position of the aryl. This led us to consider 4 sub-series of the *N*-(2-chloro-6-methylphenyl)-2-(arylamino)thiazole-5-carboxamide series (Figure 2): series 1, to interact with Glu696 and to probe for selectivity residues interactions by

introducing an amine; series 2, to engage the same residues at the pocket entrance by other chemical moieties such as fluorinated piperidines, hydroxyl groups or carboxylic acids; series 3, to examine the spatial properties of the ribose pocket by introduction of sterically demanding substituents, and series 4 to probe for dual exploitation of the pocket entrance and the ribose pocket by bulky substituents.

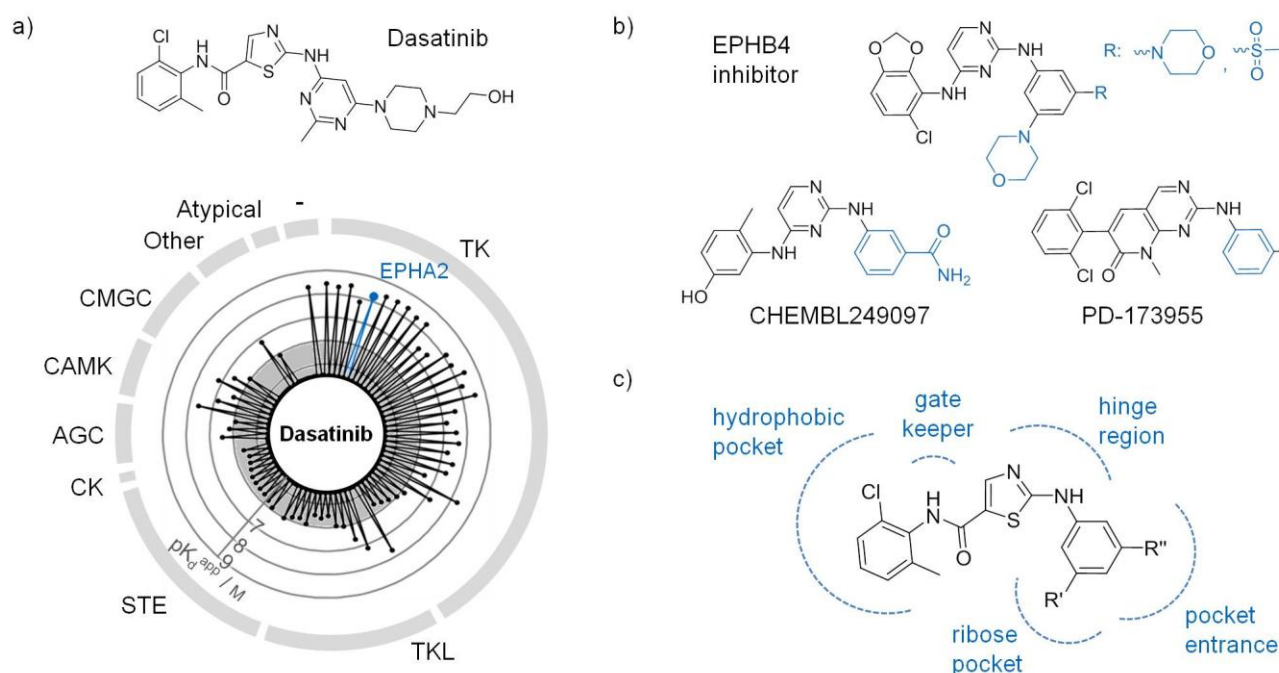


Figure 1. EPHA2 inhibitor design by hybridization of known EPH receptor binders. a) The dual BCR-ABL/SRC inhibitor Dasatinib comprises a very broad selectivity profile targeting 44 proteins with sub-micromolar affinities across several kinase families. Dasatinib is the most potent known EPHA2 inhibitor and was chosen as molecular scaffold for the development of dedicated EPHA2 inhibitors. b) Hybridization of known EPH binders (Dasatinib, EPHB4 inhibitors, CHEMBL249097, PD-173955) motivated the introduction of morpholino and methylsulfonyl moieties, the substitution of Dasatinib's pyrimidine by an aryl moiety, and the introduction of an amide bond in meta-position. c) Inhibitor design comprised a N-(2-chloro-6-methylphenyl)-2-(arylamino)thiazole-5-carboxamide scaffold binding the nucleotide binding pocket and chemical modifications which were introduced at positions R' and R'' to engage interactions within the ribose pocket and/or the ATP pocket entrance, respectively.

To obtain these four series, we synthesized the common intermediate 2-chloro-*N*-(2-chloro-6-methylphenyl)thiazole-5-carboxamide (**II**) following the procedure reported for the synthesis of Dasatinib^[27]: 2-chlorothiazole (**I**) was regioselectively metalated at position C₅ by *n*-butyllithium and the intermediate trapped with 2-chloro-6-methylphenyl isocyanate with 70-80% yield. **II** was further derivatized by acid-catalyzed nucleophilic heteroaromatic substitution with either (+)-camphor-10-sulfonic-acid (general methods A and B) or hydrogen chloride (general method C); reaction with ethyl 3-aminobenzoate yielded **III** (Method A; 66-76% yield); reaction with 5-substituted 3-aminobenzoic acids yielded **V** (Method B; 28-92% yield); reaction with 3,5-disubstituted anilines yielded **VII** (Method C; 26-34% yield). **IV** was obtained from **III** by reaction with a primary amine in the presence of DABAL-Me₃^[28] in a microwave reactor at 100-140 °C^[29] (inhibitors **1a-m**; 3-91 % yields). The amides **VI** were obtained from the carboxylic acids **V** by reaction with a primary amine and PyBroP (inhibitors **2a-i**, **3a**, **3b**; 4-74% yields). Reacting **V** with 4-aminopiperidine and HATU led to the formation of both regioisomers and reduced the yield of the desired product (**3c**, 22% yield). Compound **V** was reacted with tributyl(vinyl)tin in a palladium-catalyzed coupling reaction according to Stille to afford the carboxylic acid precursor of inhibitor **3d**. The final inhibitor was produced by coupling this precursor to 4-aminopiperidine (27% yield). Another inhibitor, **3e**, was synthesized by reacting the bromine containing inhibitor **3a** with 2-aminobenzene boronic acid in a palladium-catalyzed Suzuki coupling reaction (32% yield). Compound **VII** was afforded in an HCl-catalyzed coupling reaction by linking intermediate **II** to a 3,5-substituted aniline derivative. This aniline derivative was generated from 3,5-halogenated nitrobenzene by nucleophilic aromatic substitution at C₃ and C₅, followed by reduction of the nitro group to the primary amine. Coupling to intermediate **II** afforded the inhibitors **4a** (26% yield) and **4b** (34% yield). According to this synthesis routes, we obtained a total of 29 EPHA2 inhibitor candidates.

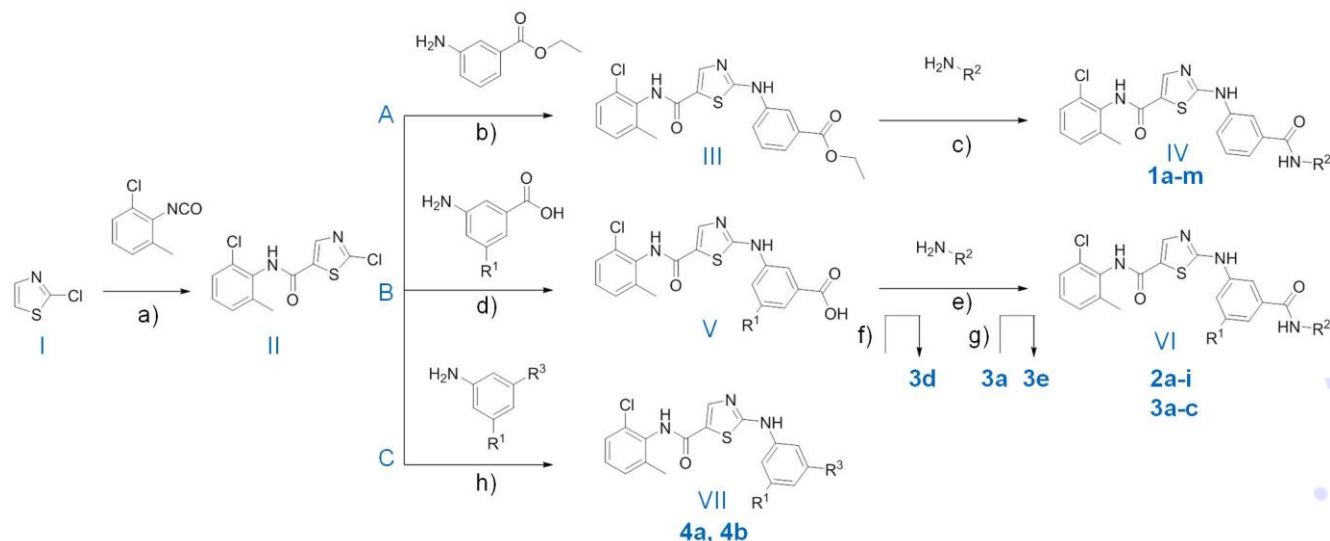


Figure 2. Synthesis scheme for EPHA2 inhibitors. a) Compound I, *n*-butyllithium, THF, -78°C , 15 min, argon; 2-chloro-6-methylphenyl isocyanate, THF, -78°C , 2h, argon (70-80% yield). b) Compound II, ethyl 3-aminobenzoate, (+)-camphor-10-sulfonic acid, 2-propanol, MW, 120°C , 3h, argon (66-76% yield). c) DABAL- Me_3 , primary amine, THF, 40°C , 30 min; Compound III, THF, MW, $100-140^{\circ}\text{C}$, 2-6 h (3-91 % yields). d) Compound II, (+)-camphor-10-sulfonic acid, 5-substituted 3-aminobenzoic acids, *tert*-butanol, MW, 120°C , 3.5 h (28-92% yield). e) Compound V, primary amine, DMF, 0°C ; DIEA, TEA, PyBroP, DMF, 30-140 min (4-74% yield). f) Compound V, tributyl(vinyl)tin, dioxane, toluene, $\text{Pd}(\text{PPh}_3)_4$, 110°C , 4h, argon (59% yield). g) Inhibitor 3a, 2-aminobenzenboronic acid, $\text{Pd}(\text{PPh}_3)_4$, DMF; K_2CO_3 , MW, 115°C , 5h, argon (32% yield). h) 3,5-substituted aniline, 2-propanol, compound II, HCl, ON, 95°C (26-43%).

EPHA2 inhibitors bind EPHA2 with high affinity

We determined the affinity of all 29 inhibitor candidates by single dose competitive Kinobeads^[21, 22] pulldowns (Supplementary Figure 2) coupled to either quantitative Western Blotting (10 μM compound concentration, Supplementary Figure 3) or mass spectrometry read out (3 μM compound concentration) to calculate the relative binding inhibition of EPHA2 compared to a DMSO control (Table 1). The results reveal that inhibitors targeting charged residues at the ATP pocket entrance by an amine (**1a-m**; 40-95% binding inhibition), a hydroxyl group (**2d-f**; 43-67% binding inhibition) or a carboxyl group (**2g-l**; 40-93% binding inhibition) showed varying binding inhibition of EPHA2. The most promising candidates

presenting binding inhibitions of more than 90% contained either a secondary amine (**1g**: 95%, **1l**: 94%) or a carboxylic acid functional group (**2h**: 93%, **2i**: 93%). For further inhibitor development, the piperidine moiety of inhibitor **1g** was favored over the other modifications as it was the only one without chiral center. The modifications introduced at R' (Figure 1c) allowed us to investigate the spatial properties of the ribose pocket using groups of increasing steric hindrance (inhibitors **3a-e**, **4a-b**). Inhibitor **3e** comprising an aniline moiety showed high binding inhibition (96%) which indicated that larger hydrophobic groups potentially establishing hydrophobic interactions are tolerated at this position. Inhibitors **4a** and **4b** contain a morpholine or methylsulfonyl group as substituents pointing towards the ribose pocket and showed similar behavior with very high binding inhibition of 98% and 95%, respectively. The inhibitory activity of selected compounds (**2c**, **2f**, **2i**, **4b**) was confirmed by recombinant activity assays, establishing that the Kinobeads binding assay can indeed aid in discovering functional inhibitors of EPHA2 (Table 2).^[30]

Novel EPHA2 inhibitors display improved selectivity

To investigate whether the new inhibitors would be more selective for EPHA2 than the parent lead compound Dasatinib, we subjected 16 compounds to full dose response measurements using Kinobeads with quantitative mass spectrometry readout (Supplementary Table). The addition of increasing concentrations of an inhibitor to lysates of cancer cells in a competitive pulldown setup will lead to a concentration-dependent decrease of compound binding to the beads and thus the mass spectrometric intensity. This approach allows determination of an apparent dissociation constant K_d^{app} for all drug-protein interactions. As mentioned earlier, Dasatinib bound 44 targets with sub-micromolar affinity (Figure 3a). In contrast, all novel EPHA2 inhibitors had fewer sub-micromolar targets ranging from 13 (inhibitor **2g**) to 31 (inhibitor **4a**). Closer inspection of the target profiles revealed decreased affinities and fewer targets in all kinase groups, but particularly in the TK, TKL, STE and AGC branches. Interestingly, for many of our inhibitors we observed substantially reduced binding affinities for members of the SRC family of kinases (SRC, YES1, FYN, LCK, LYN, HCK, FRK) which are among the main targets of the designated dual ABL/SRC inhibitor Dasatinib. We then sought to quantify the selectivity of the inhibitors. Different metrics have been developed for this purpose including the selectivity score^[31], the gini coefficient^[32] and the selectivity entropy^[33]. However, they all suffer from different drawbacks

such as dependence on the number of kinases tested in the experiment, negligence of binding affinities or non-protein centric selectivity calculation. Therefore, we developed a novel scoring system called *concentration and target dependent selectivity* (CATDS; Supplementary Figure 4a) which enabled us to overcome these limitations and to calculate drug selectivity for a certain target of interest (here: EPHA2) in a concentration-dependent manner (here: at the K_d^{app} of EPHA2). This approach is of benefit in a medicinal chemistry program to evaluate the difference in selectivity of several inhibitors in the light of a particular target protein. CATDS adopts values between 0 (unselective) and 1 (selective) and can be interpreted as the percentage of an applied compound that binds to a particular target at a particular concentration. Here, simple target counting without consideration of the affinities towards EPHA2 or the other targets would identify inhibitor **2g** (13 targets below 1 μ M) as most selective inhibitor (Figure 3b, upper panel). This interpretation would, however, be misleading because the compound is also the weakest of all the inhibitors (K_d^{app} (EPHA2): 3.4 μ M). In contrast the CATDS score highlighted inhibitors **4a** (CATDS_{EPHA2}: 0.176, K_d^{app} (EPHA2): 0.8 nM) and **2c** (CATDS_{EPHA2}: 0.141, K_d^{app} (EPHA2): 2 nM) to be the most selective EPHA2 inhibitors in the panel (Figure 3b, lower panel, Table 2, Supplementary Figure 4b for comparison with other selectivity metrics). Even though inhibitor **2g** only bound 13 proteins and inhibitor **4a** targeted 31 proteins at a concentration arbitrarily set to 1 μ M, the latter is still the more selective compound as it engages fewer drug-protein interactions at the K_d^{app} of EPHA2 (Figure 3c, Supplementary Figure 5 for radar plots of all inhibitors). In our opinion, it is important to consider the dose dependence of compound selectivity because it can guide the choice of dose in a biological system.

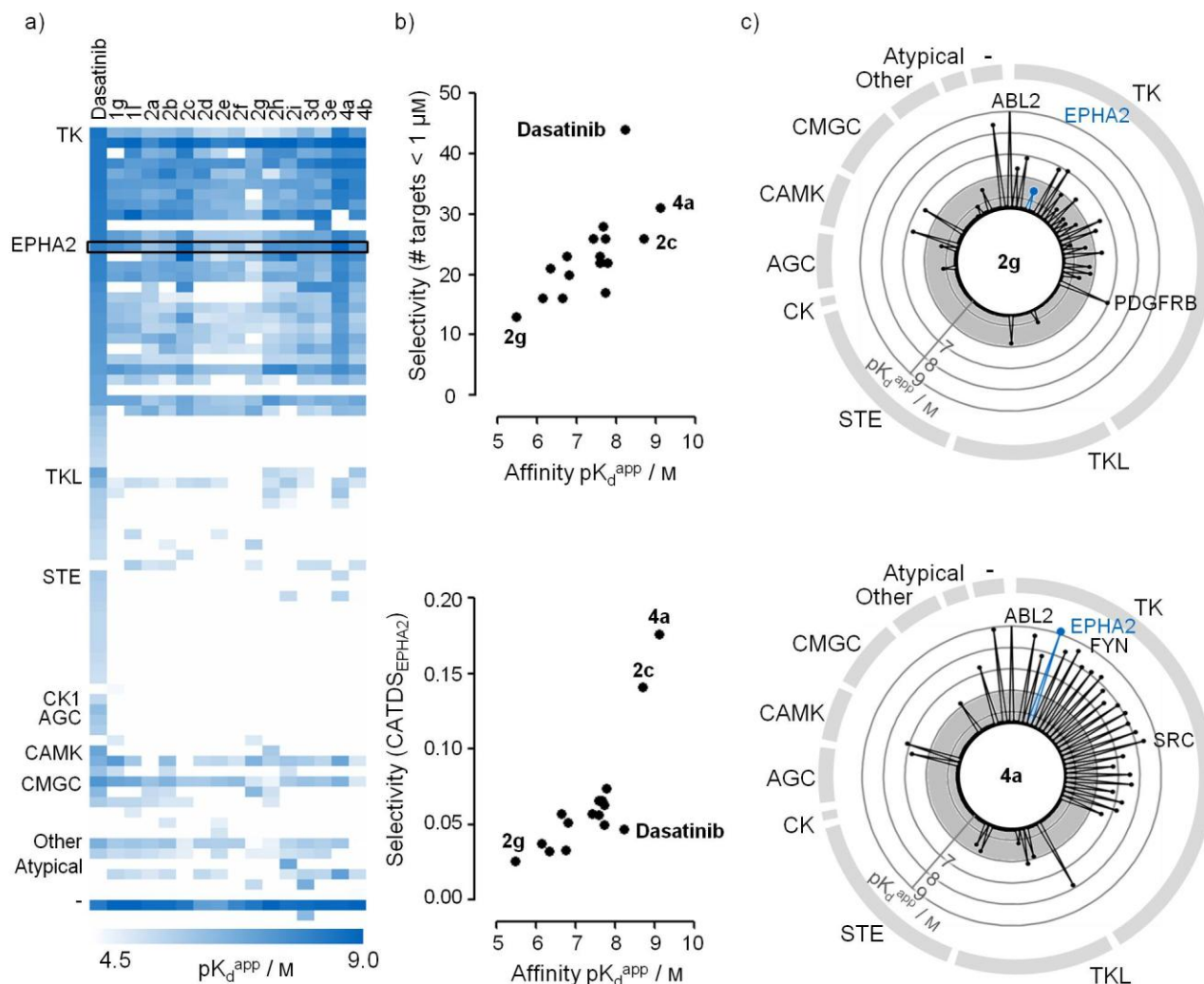


Figure 3. Selectivity profiles of EPHA2 inhibitors. a) Heatmap showing selectivity profiles and apparent binding affinities (pK_d^{app} [M]) of Dasatinib and EPHA2 inhibitor candidates. Target kinases are sorted according to kinase phylogeny. EPHA2 is highlighted by a black box. b) Selectivity of EPHA2 inhibitors as obtained by simple target counting (upper panel) or the EPHA2-specific CATDS_{EPHA2} score (concentration and target dependent selectivity, lower panel). Inhibitor **4a** was found to be the most potent and most selective EPHA2 inhibitor in our panel. c) Radar plots depicting the target space and binding affinities of inhibitor **2g** which showed the lowest number of targets but also lowest affinity for EPHA2 (upper panel), and inhibitor **4a** that has the highest affinity and selectivity for EPHA2 (lower panel).

Protein crystallography validates two major pockets for interaction with EPHA2 inhibitors

We performed co-crystallization experiments of 17 EPHA2 inhibitors and recombinant EPHA2 kinase domain (Asp596-Gly900) expressed in Sf9 cells (Table 2).^[34] As anticipated, all inhibitors bound to the ATP binding site in the typical type 1 (DFG-in) conformation, and the *N*-(2-chloro-6-methylphenyl)-2-(methylamine)thiazole-5-carboxamide part of the molecule – common to all inhibitors, including Dasatinib – was equally positioned in all inhibitor-EPHA2 co-crystals (Figure 4a). The direct interactions to residues Met667, the gatekeeper Thr692 and Met695 (hinge region) as previously reported for Dasatinib were also maintained. More interestingly, an overlay of all obtained structures showed that the inhibitors engaged the pocket entrance as well as the ribose pocket as originally intended (Figure 4b). We noticed that residues R' and R'' do not adopt similar conformations in the different crystal structures but distribute across the pockets. As observed e.g. for inhibitor **2c**, the aryl moiety could adopt different rotational poses leading to the R' moieties to target either of the two pockets. Inhibitors **1a-m**, **2a-i** and **3a-e** contain an amide linkage and we observed that this additional moiety, as compared to Dasatinib, was engaged in binding interactions with the target in the majority of inhibitors. The interaction was mostly established with Glu696 located in the hinge region, as intended by our hybrid design (Figure 4c, 11 molecules out of 15). In addition to Glu696, the amide bond also engaged Tyr694 via direct side chain interaction (e.g. inhibitors **2f-g**). Unexpectedly, we found that the amide bond orientation was very flexible and could also form backbone interactions with Ile619 and Ala699 within the ribose pocket (e.g. inhibitors **2e**, **1l**). Targeting what we expected to be “selectivity residues” also proved successful, since some amine, hydroxyl or carboxyl functional groups, which we positioned in different spatial orientations, were able to extend the molecular interactions to the charged residues Lys617, Glu706 and Lys702 located at the entrance of the ATP pocket (Figure 4d). Inhibitors carrying an amine often engaged Glu706 and Lys702 in a water-mediated interaction (e.g. inhibitors **1g**, **2a**, **3e**, **3b**, **3d**). Lys617 located in the N-lobe was targeted by a primary amine (inhibitor **1j**). The carboxyl containing inhibitor **2g** looped back towards the ATP pocket to interact with Tyr694. Molecules **2d** and **2e** comprising a hydroxyl group unexpectedly engaged the ribose pocket which positioned the hydroxyl group in an orientation distant to the target residues, whereas the hydroxyl group of molecule **2f** directly interacted with Glu706 with a distance of 2.5 Å. As expected, direct interactions within the ribose pocket were scarce and inhibitor-EPHA2 interaction in this binding site was mainly driven by hydrophobic contacts and advantageous space-filling with sterically demanding groups (e.g. inhibitors **3e**, **4a**). Interestingly, inhibitor **3b** features a precise symmetric orientation of its trifluoro group towards the carbonyl oxygen of the Ile619 backbone. Due to the strong electronegativity of oxygen, CF⁻-O

interactions are typically known to be of rather repulsive than attractive nature.^[35] However, the carbonyl oxygen directly points towards the positively polarized C atom of the CF₃ unit. It is therefore tempting to speculate that this might positively affect inhibitor binding. Inhibitor **4a** was found to be the most affine (K_d^{app} : 0.8 nM) and most selective inhibitor for EPHA2 (CATDS_{EPHA2}: 0.176, i.e. 17.6% of **4a** bound to EPHA2, which is 4 times more than Dasatinib). Somewhat surprisingly, it did not engage in additional direct interactions but occupied both the ATP entrance as well as the ribose pocket. We hypothesize that occupying both pockets with the same residue reduces degrees of freedom and therefore favors inhibitor binding due to entropic contribution.

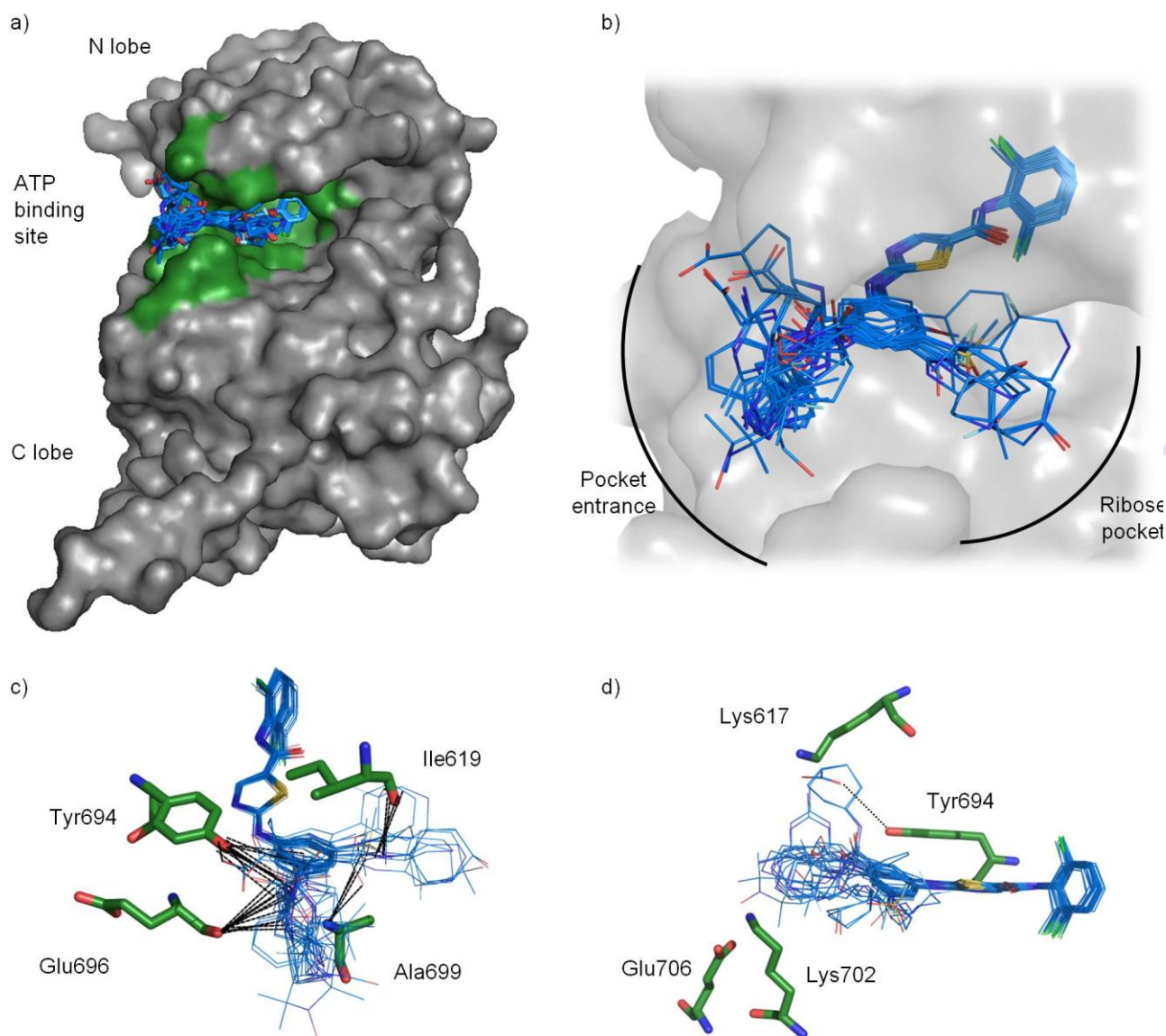


Figure 4. Inhibitor-EPHA2 co-crystal structures validate medicinal chemistry concept. a) All 17 EPHA2 inhibitor candidates bound in the type 1 conformation (DFG-in) in the ATP binding site located between the N lobe and the C lobe. b) The inhibitors engaged both, the ATP pocket entrance and the ribose pocket. c) In most inhibitors, the introduced amide bond formed direct side chain interactions with Tyr694 and Glu696 located towards the ATP pocket entrance. In some inhibitors, another conformation involving backbone interactions to Ile619 and Ala699 in the ribose pocket was observed. d) As intended, selectivity residues Lys617, Lys702, Glu706 were often engaged in direct or water-mediated interactions by inhibitors carrying an amine, hydroxyl or carboxyl group. Surprisingly, inhibitor **2g** carrying a carboxylic moiety adapted an unexpected bent conformation and interacted with Tyr694 (indicated by dashed line).

Cellular activity of EPHA2 inhibitors in SF-268 cells

We examined the anti-proliferative potential of the EPHA2 inhibitor candidates in a human cancer cell line that is growth-dependent on EPHA2. In order to identify a cellular system that would be specifically suitable for testing our inhibitor panel, we used kinome-wide protein expression profiling data of the NCI60 panel of cancer cell lines previously obtained using the Kinobeads technology.^[36] A suitable cell line was defined as featuring high EPHA2 expression and low abundance of other kinases targeted by the EPHA2 inhibitors. As mass-spectrometry intensities are biased by the affinity of the Kinobeads for the different kinases, we chose to determine the expression change of the proteins across the NCI60 panel relative to the mean protein intensity level (z-score transformation). The resulting value depicts the number of standard deviations by which the protein intensity in a particular cell line differs from the mean intensity across the panel and indicates relative high (positive values) or low (negative values) abundance of a protein. In the literature, the prostate cancer cell line PC-3 is often used as EPHA2 dependent cellular system. However, for testing our EPHA2 inhibitors this cell line was found to be non-advantageous as it revealed high expression levels of several other prominent targets of our inhibitors, such as ABL1, SRC, YES1 and other EPH inhibitors (e.g. EPHB4, EPHB2, EPHA5). The glioblastoma cell line SF-268 showed the highest EPHA2 expression level among the NCI60 panel and also featured an advantageous overall kinome profile (Figure 5a). We combined all 77 proteins identified as targets of all EPHA2 inhibitors generated in this study as well as Dasatinib and sorted them according to the

maximum observed affinity, regardless of which inhibitor showed this affinity (pK_d^{app} , Figure 5a, black dots). Target proteins that bound with high affinity were targeted by a large proportion (> 80 %) of the dedicated EPHA2 inhibitors (Figure 5a, bar color). The distribution of relative intensities (Figure 5a, bar chart) revealed that almost all potentially inhibited targets other than EPHA2 – as for example the main targets of Dasatinib ABL and SRC – are relatively weakly expressed in this cell line compared to all other cell lines of the NCI60 panel. Within a therapeutic window of 10 (indicated by the dark grey box), only EPHA4 and FYN show slightly higher expression and may thus be candidates for relevant off-targets in this cell line. Within a therapeutic window of 100 (indicated by the light grey box) only DDR2 was another such candidate. Western blot analysis of SF-268 cells showed that this cell line expresses phosphorylated EPHA2 (at S897) and AKT1 (at S473) which is indicative for aberrant and tumor-promoting ligand-independent EPHA2 signaling (Supplementary figure 6).^[37] Next, protein knockdown experiments by siRNA were performed to demonstrate a functional dependence of SF-268 cell viability on EPHA2 expression (Figure 5b). Four independent siRNAs were examined separately and as a mixture and revealed a reduction of cell viability of about 60% after 6 days of treatment. From these results, we deduced that SF-268 cells are suitable for testing EPHA2-directed inhibitors and that cell viability reduction is an appropriate readout for assessing the response of the cell to EPHA2 inhibition.

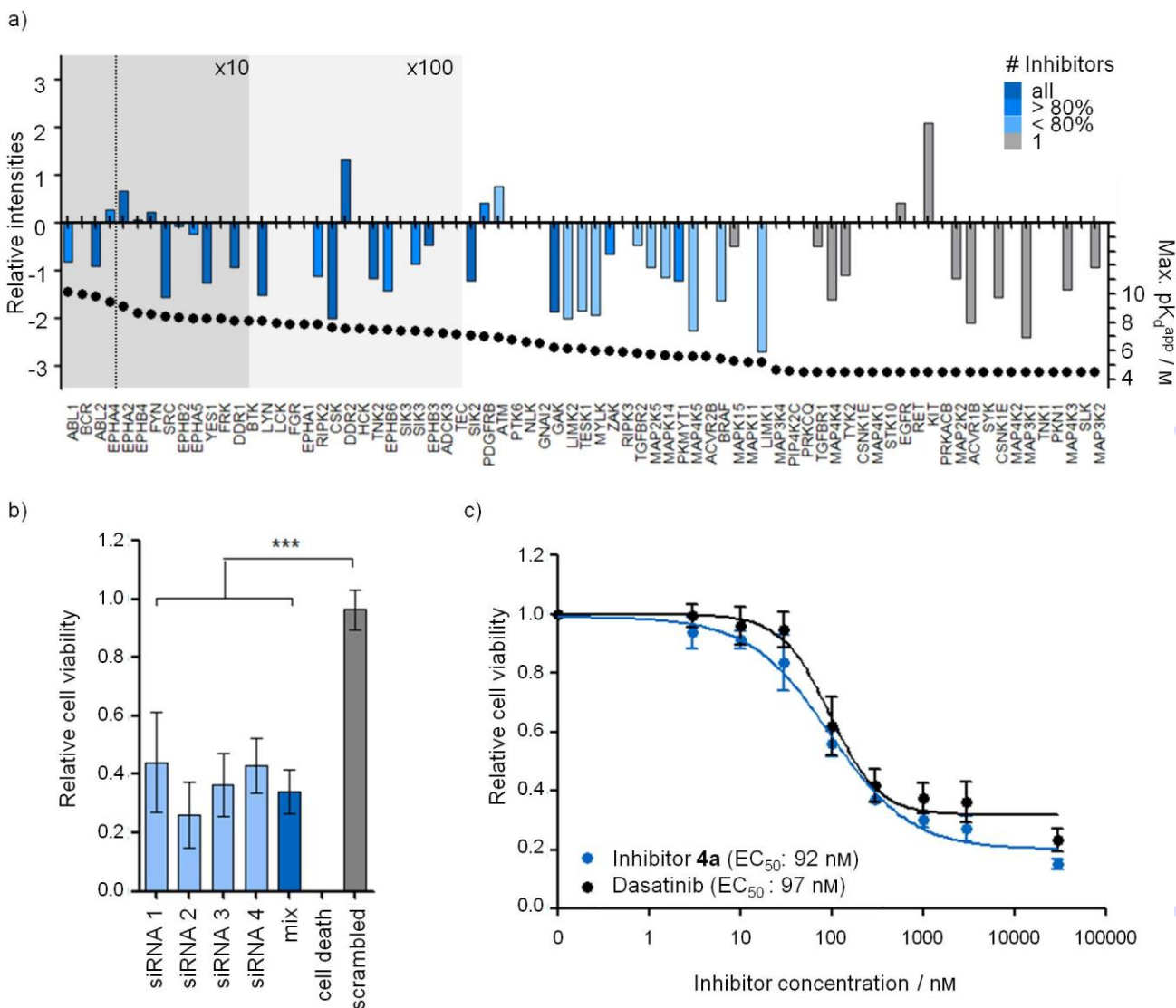


Figure 5. Inhibitor 4a shows anti-proliferative effects in the SF-268 glioblastoma cell line. a) Kinome profiling of the NCI60 panel of cancer cell lines revealed that SF-268 cells feature high EPHA2 expression and low abundance of other targets (bar chart) frequently hit by our EPHA2 inhibitors (bar color). Inhibitor targets were sorted according to the maximum observed affinity (pK_d^{app} [M]) within our dataset and theoretical therapeutic windows were set at 10x and 100x K_d^{app} of EPHA2. b) Protein knockdown of EPHA2 by four independent siRNAs confirmed that SF-268 cell viability is dependent on EPHA2 expression. Experiments were performed in three biological replicates each containing three technical replicates. Significance was calculated by a two-sided unpaired student's t-test. c) SF-268 cells were treated with increasing concentrations of inhibitor **4a** resulting in potent reduction of cell viability similar to Dasatinib.

EPHA2 inhibitor **4a** potently reduces SF-268 cell viability

Having established the glioblastoma cell line SF-268 as a suitable biological model, we measured the anti-proliferative effect of the inhibitor candidates synthesized in this study. Cellular activity was examined utilizing a resazurin-based cell viability assay where reduced metabolic activity of cells leads to decreased reduction of resazurin to resorufin. Inhibitor treatment was performed in full dose response experiments with eight inhibitor concentrations ranging from 3 nM to 30 μ M. Most of the compounds inhibited cell viability with low micromolar potency (**2c**: 1.4 μ M – **1g**: 4.4 μ M, Table 2), whereas inhibitors **2g-i** did not show any anti-proliferative effect. We attribute the latter to the presence of a charged carboxyl moiety that likely impairs cellular uptake. Future work on these compounds will therefore include derivatization into ester prodrugs with enhanced permeability. Inhibitor **1g** bearing a piperidine at position R' affected SF-268 cell viability with a very low potency of 4.4 μ M. This result can be rationalized by comparison to meta-fluorinated versions of this compound (inhibitors **2a-2c**). Cellular potency increased 2- to 3-fold for the singly fluorinated (EC_{50} (**2a**): 1.99 μ M, EC_{50} (**2b**): 1.54 μ M) and doubly fluorinated inhibitor **2c** (EC_{50} : 1.4 μ M). This indicates that the positive charge of the piperidine at physiological pH (pK_a of around 11) could be responsible for the diminished cellular effect of inhibitor **1g**. Indeed, fluorination in meta-position to the secondary amine should reduce the pK_a of piperidine from 11 to 9 (singly fluorinated) and 7 (doubly fluorinated) and the obtained molecules showed more activity in the viability assay. Interestingly, inhibitors **4a** and **4b** were much more potent (**4a**: 92 nM, **4b**: 506 nM) and similar to the potency of the lead compound Dasatinib (97 nM) (Figure 5c). While we cannot entirely rule out that this potency can only be attributed to the inhibition of EPHA2, this excellent activity designated **4a** as the most promising EPHA2 inhibitor in our current compound set with a strong demonstrated anti-proliferative effect in a relevant EPHA2 overexpressing cell line.

Conclusions

In this study, we have demonstrated the utility of a chemoproteomics-aided medicinal chemistry approach for the successful discovery of EPHA2 inhibitors based on a clinically used drug as a lead structure. Our currently best compound inhibitor **4a** shows an improved selectivity profile compared to Dasatinib making it a more suitable chemical tool for the study of EPHA2 related disease biology. We will continue to work on **4a** and related compounds but will also provide the compound to interested researchers in order to better characterize its properties and to further develop its potential not only for oncology but also in infectious diseases. We also point out here that the chemoproteomic approach to guiding medicinal chemistry presented here should be more generally applicable and could develop into a valuable strategy for drug discovery in the future.

Experimental section

Cell lines and reagents. K-562, MV-4-11 and COLO 205 cells were cultivated in RPMI medium 1640 (RPMI1640, Biochrom GmbH) and SK-N-BE(2) was grown in Dulbecco's modified Eagle medium/Ham's F12 (DMEM/F12, Biochrom GmbH), all supplemented with 10% (v/v) fetal bovine serum (Biochrom GmbH) and 1% antibiotic/antimycotic solution (Sigma Aldrich). SF-268 cells were grown in Iscove's Modified Dulbecco's Medium (IMDM, Biochrom GmbH) supplemented with 10% (v/v) fetal bovine serum. Cell lines were kindly provided by the NCI-Frederick Cancer DCTD Tumor/Cell line repository, were not found in the database of commonly misidentified cell lines (ICLAC) and were tested negatively for mycoplasma contamination. Cell lysis and Bradford assay were performed as described previously.^[22, 23] Kinase affinity matrices were prepared in house as published elsewhere.^[22, 23]

Selectivity profiling with kinase affinity matrices. 96-well plate Kinobeads competition assays have been performed as described previously.^[22, 23] Briefly, 5 mg mixed protein lysate (K-562, MV-4-11, SK-N-BE(2) and COLO 205) was pre-incubated with compound dilutions in DMSO (0, 3, 10, 30, 100, 300, 1000, 3000, 30000 nM final concentrations) for 45 min at 4 °C. Subsequently, lysate was incubated with 35 µl settled and equilibrated Kinobeads for 30 min at 4 °C. DMSO control lysate was recovered for the pulldown of pulldown experiment. Beads were washed and bound proteins were eluted with 40 µl 2x LDS sample buffer (NuPAGE, Invitrogen) containing 50 mM DTT. Reduced disulfide bridges were alkylated using 4 µl chloroacetamide (55 mM). Proteins were concentrated and desalted by a short SDS-PAGE using a 4-12% gel (NuPAGE, Invitrogen) and in-gel digested according to standard procedures.

Immunoblot analysis. Antibodies against EPHA2 (C20, sc-924), EPHA2 pS897 (#6347), AKT1 (#4691), AKT1 pS473 (#4060), α -tubulin (E-19, sc-12462), β -Actin (C4, sc-47778) were purchased from Santa Cruz or Cell Signaling technology. Half of the obtained Kinobead eluate or 120 µg cell lysate was separated by 4-12% NuPAGE gel electrophoresis and transferred onto PVDF membranes (Novex, Life Technologies). Membranes were blocked for 1 h in 2% BSA in 1x Tris buffered saline at room temperature and probed over night at 4 °C with the respective primary antibody. Antibody binding was detected using fluorophore-conjugated secondary antibodies (LI-COR) in an Odyssey scanner (LI-COR Biosciences).

LC-MS/MS analysis. Peptides generated by in-gel trypsin digestion were analyzed via LC-MS/MS on a nanoLC-Ultra 1D+ (Eksigent) coupled to a LTQ-Orbitrap Elite mass spectrometer (Thermo Scientific) as described previously.^[22, 23] Peptides were delivered to a trap column (100 µm x 2 cm, packed in house

with Reprosil-Pur C18 AQ 5 μm resin, Dr. Maisch) for 10 min at a flow rate of 5 $\mu\text{L}/\text{min}$ in 100% solvent A₀ (0.1% v/v FA in HPLC grade water). Peptides were then separated on an analytical column (75 μm x 40 cm, packed in-house with Reprosil-Gold C18, 3 μm resin, Dr. Maisch) using a 100 min gradient ranging from 4-32% solvent B (0.1% v/v FA and 5% v/v DMSO in acetonitrile) in A (0.1% v/v FA and 5% v/v DMSO in HPLC grade water) at a flow rate of 300 nL/min. The mass spectrometer was operated in data dependent mode, automatically switching between MS and MS2 spectra. Up to 15 peptide precursors were subjected to fragmentation by higher energy collision-induced dissociation (HCD) and analyzed in the Orbitrap. Dynamic exclusion was set to 20 s. A kinase peptide inclusion list (3 most intense peptides per kinase) was enabled.

Peptide and protein identification and quantification. Label free quantification was performed using MaxQuant (version 1.5.3.30)^[38] by searching MS2 data against all canonical protein sequences as annotated in the Swissprot reference database (human proteins only, 20,193 entries, downloaded 22.03.2016, internally annotated with PFAM domains) using the embedded search engine Andromeda^[39] as described previously.^[22, 23] Carbamidomethylated cysteine was used as fixed modification; variable modifications included phosphorylation of serine, threonine or tyrosine, oxidation of methionine, and N-terminal protein acetylation. Trypsin/P was specified as proteolytic enzyme with up to two allowed missed cleavage sites. Precursor and fragment ion tolerances were 10 ppm and 20 ppm, respectively. Label-free quantification^[40] and match-between-runs options were enabled and results were filtered for a minimal length of seven amino acids, 1% peptide and protein FDR as well as common contaminants and reverse identifications. For consistent peptide identification and protein grouping, the MS data for each compound was supplemented with 15 standard DMSO controls. Each compound was analyzed separately.

Data analysis and visualization. LFQ intensities were normalized to DMSO controls and EC₅₀ values were deduced by a four-parameter log-logistic regression using an in-house pipeline based on the drc add-on package in R.^[41] The depletion factor was calculated and applied to transform EC₅₀ to K_D^{app} values as described previously.^[22, 23] Binding affinities are reported as pK_D^{app} values which is the negative logarithm (base 10) of the K_D^{app} value in mol/L. For the calculation of the selectivity score S a threshold was set at 10 times K_D^{app} (EPHA2), the number of kinase targets was counted and divided by all identified protein kinases as a reference.^[31] Gini coefficient was calculated using the K_D^{app} (EPHA2) of the respective compound as threshold concentration.^[32] Figures and tables were produced in GraphPad Prism 5 (version 5.01) and Excel.

NCI60 kinome profiling. NCI60 kinome data were obtained from Gholami *et al* ^[36] and processed in MaxQuant (version 1.4.0.5) applying the same settings as above and including iBAQ quantification. MaxQuant results were analyzed using the MaxQuant associated software suite Perseus (version 1.5.6.0). ^[42] iBAQ intensities were log2 transformed and normalized by protein-wise Z-score transformation.

Protein knockdown by small interfering RNA (siRNA). SF-268 cells were seeded in 96-well plates (1000 cells per well), incubated for 24 h and medium was exchanged before addition of siRNA (Qiagen: SI00063553, SI0030081, SI00300188, SI02223508). siRNA was diluted in Opti-MEM medium (Gibco, Life Technologies) to a concentration of 70 nM. Upon addition of INTERFERin™ (PolyPlus, peqlab), the mixture was vortexed for 10 s and incubated at room temperature for 10 min before addition to the cells at a final concentration of 20 nM. The different siRNA preparations were tested individually and as mix of all four siRNA. Controls were performed using 1 nM AllStars scrambled (Qiagen, SI03650318) and CellDeath siRNA (Qiagen, SI04381048), INTERFERin™ only and Opti-MEM medium only. Cell viability was determined according to the manufacturer after 6 days by fluorescence readout of alamarBlue (Pierce) in a FluoStar Omega plate reader (excitation: 544 nm, emission: 590 nm). All experiments were repeated in technical triplicates and biological triplicates. Relative cell viability was normalized to the INTERFERin control. Statistical analysis was performed using an unpaired two-tailed t-test (significance level $p < 0.001$).

Kinase inhibitor treatment. SF-268 cells were seeded in 96-well plates (1000 cells per well) and incubated for 24 h before treatment. Drug dilutions were prepared in DMSO (0, 3, 10, 30, 100, 300, 1000, 3000, 30000 nM final concentrations) and added to the cells to a final DMSO concentration of 0.3%. Cells were incubated with drug for 72 h and cell viability was determined according to the manufacturer by fluorescence readout of alamarBlue (Pierce) in a FluoStar Omega plate reader (excitation: 544 nm, emission: 590 nm). Drug treatments were performed in biological replicates each containing three technical replicates.

Kinase activity assay. Dose dependent inhibition of EPHA2 kinase activity was validated for selected inhibitors by a radioactive filter binding assay provided by Reaction Biology as published previously. ^[43]

Docking. The binding poses of Dasatinib, CHEMBL249097 and PD-173955 in the ATP-binding site of EPHA2 were predicted by molecular docking using Glide (Schrödinger, Inc.). The crystal structure of EPHA2 in complex with ANP was retrieved from the Protein Data Bank (PDB: 1MQB) and prepared using the Protein Preparation Wizard in Maestro (Schrödinger, Inc.) to remove non amino acid molecules, add

hydrogen atoms, and assign the protonation states for the polar residues. The scoring grid was generated by enclosing the residues 14 Å around Dasatinib in the binding site. The docking was performed in Glide SP mode and the top ranked pose by GScore of each inhibitor was retained for visual analysis of interactions.

Recombinant expression and purification of EPHA2 kinase domain. The detailed protocols for isotopic labeling procedures, expression and purification conditions of EPHA2 were published elsewhere.^[34] In brief, the gene encoding the catalytic domain of human EPHA2 (residues D596-G900) was synthesized at GenScript USA Inc., USA and was optimized for its expression in insect cells. Synthesized EPHA2 gene was sub-cloned in pTriEx 1.1 with cleavable N-terminal Flag-His tag. Recombinant baculovirus incorporating the kinase cDNA construct was generated by homologous recombination with BacMagic DNA (Novagen), in *Spodoptera frugiperda* (Sf9) cells. High titer viral stocks were generated by infection of Sf9 cells, which were then used for the expression of EPHA2 by infection of Sf9 cells in large-scale. Recombinantly expressed EPHA2 was isolated from the cellular extracts by passage over NiNTA resin, followed by removal of Flag-polyhistidine tags with TEV protease (in-house) and inverse NiNTA. The protein was further purified by size-exclusion chromatography with 20 mM Tris, 0.2 M NaCl, 5 mM MgCl₂, 3 mM TCEP, the peak fractions were concentrated to 9.4 mg/ml and stored at –80 °C. Purified EPHA2 was not phosphorylated during the expression in Sf9 cells and isolation procedures, as determined by mass spectrometry.

Protein crystallization and structure determination. Purified EPHA2 protein was concentrated up to 6–10 mg/ml in a buffer containing 20 mM Tris-HCl pH 8.0, 200 mM NaCl, 5 mM MgCl₂ and 3 mM TCEP. After the addition of different ligands up to a final concentration of 1 mM, the protein sample was diluted 1:1 with crystallization buffer in crystallization drops of 500–800 nl volume on a 96-well microplate. Crystals were grown as sitting drops at 291 K against 50 µl reservoir solution. Rod-shaped crystals (0.1–0.2 mm) or plate-like cuboids (0.05–0.1 mm) appeared after 1–2 weeks and grew to their final size within 4 weeks. Crystallization conditions were composed from three different building blocks and varied for each ligand between the following ranges: 30–40% precipitant solution (stock solution consisting of 25% PEG 1000, 25% PEG 3350, 25% MPD), 0.05–0.3 M amino acids solution (stock solution consisting of 0.2 M glutamate, 0.2 M glycine, 0.2 M serine, 0.2 M alanine, 0.2 M lysine) or 0.05–0.3 M carboxylic acids solution respectively (stock solution consisting of 0.2 M sodium formate, 0.2 M ammonium acetate, 0.2 M sodium citrate, 0.2 M sodium/potassium tartrate, 0.2 M sodium oxamate) and 0.1 M buffer pH 5.5–8.5 (Bis-Tris, Tris, Hepes, MES, Bicine or Tris/Bicine). Prior to flash-cooling some crystals had to be

soaked with 20% ethylene glycol in mother liquor for cryoprotection. Diffraction data at resolutions between 1.10–1.89 Å had been collected at beamline BL14.1 operated by the Helmholtz-Zentrum Berlin (HZB) at the BESSY II electron storage ring (Berlin, Germany)^[44] at beamline P13 operated by the EMBL Hamburg at the PETRA III synchrotron source (DESY, Hamburg Germany)^[45], at X06DA (PXIII) beamline operated by the Swiss Light Source (PSI, Villigen, Switzerland) and at PROXIMA-1 beamline operated by the Synchrotron SOLEIL (Saint-Aubin, France). The data was processed using *XDSAPP*.^[46] The structure was determined by molecular replacement with *Phaser*^[47] using the crystal structure of the human EPHA2 kinase domain (PDB: 5I9Y)^[20] as a search model. Model building was performed using *Coot*^[48] and the structure was refined and validated using *PHENIX*.^[49] Drug-protein interaction analysis was performed using LigPlot+.^[50] Figures containing molecular graphics were prepared using *PyMOL* (Schroedinger). Structure-solution and refinement statistics can be found in Supporting Information.

Data deposition. Structural data is accessible via PDB protein data bank: inhibitor 1g (pdb: 5NJZ), inhibitor 1j (pdb: 5NK0), inhibitor 1k (pdb: 5NK1), inhibitor 1l (pdb: 5NK3), inhibitor 1m (pdb: 5NK5), inhibitor 2a (pdb: 5NK7), inhibitor 2c (pdb: 5NK4), inhibitor 2d (pdb: 5NK6), inhibitor 2e (pdb: 5NK9), inhibitor 2f (pdb: 5NK8), inhibitor 2g (pdb: 5NKA), inhibitor 3a (pdb: 5NKE), inhibitor 3b (pdb: 5NKF), inhibitor 3d (pdb: 5NKG), inhibitor 3e (pdb: 5NKH), inhibitor 4a (pdb: 5NKB), inhibitor 4b (pdb: 5NKI). The mass spectrometry data and all obtained dose response curves for each inhibitor selectivity profiling have been deposited to the ProteomeXchange Consortium (<http://proteomecentral.proteomexchange.org>) via the PRIDE partner repository^[51] with the dataset identifier PXD006193.

Acknowledgements

Diffraction data were collected on BL14.1 at BESSY II (Helmholtz-Zentrum Berlin), on beamline P13 at PETRA III (EMBL Hamburg), on X06DA (PXIII) beamline at the Swiss Light Source (Paul Scherer Institute) and at PROXIMA-1 beamline operated by the Synchrotron SOLEIL (Saint-Aubin, France). The presented research was in parts funded by the German Consortium for Translational Cancer Research (DKTK), the German Cancer Research Center (DKFZ), Heidelberg, Germany and the European Community's Seventh Framework Programme (FP7/2007-2013) under the BioStruct-X (grant agreement N283570). H.S. is member of the DFG cluster of excellence: macromolecular complexes. BMRZ is supported by the state of Hessen. B.K. is a member of the DFG cluster of excellence: Center for Integrated Protein Science Munich (CIPSM). The authors want to thank Susan Klaeger, Runsheng Zheng and Dongxue Wang for mass-spectrometric measurements and Huichao Qiao for production of cell lysates. The authors also want to thank Andrea Hubauer, Michaela Krötz-Fahning and Andreas Klaus for technical assistance and Jonas Goldstein for LigPlot+ analysis. The authors thank the members of the Chair of Food Chemistry and Molecular Sensory Science (Prof. Hofmann) and the Chair of Biochemistry (Prof. Eisenreich, Prof. Groll) at the Technical University of Munich for NMR measurement.

Keywords: chemical proteomics, drug discovery, EPH receptor, inhibitors, selectivity profiling

References

- [1] A. Barquilla, E. B. Pasquale, *Annu Rev Pharmacol Toxicol* **2015**, *55*, 465-487.
- [2] A. C. Andres, H. H. Reid, G. Zurcher, R. J. Blaschke, D. Albrecht, A. Ziemiecki, *Oncogene* **1994**, *9*(5), 1461-1467.
- [3] J. E. Park, A. I. Son, R. Zhou, *Genes (Basel)* **2013**, *4*(3), 334-357.
- [4] Z. Wu, J. B. Doondea, A. M. Gholami, M. C. Janning, S. Lemeer, K. Kramer, S. A. Eccles, S. M. Gollin, R. Grenman, A. Walch, S. M. Feller, B. Kuster, *Mol Cell Proteomics* **2011**, *10*(12), M111.011635.
- [5] M. L. Taddei, M. Parri, A. Angelucci, B. Onnis, F. Bianchini, E. Giannoni, G. Raugei, L. Calorini, N. Rucci, A. Teti, M. Bologna, P. Chiarugi, *Am J Pathol* **2009**, *174*(4), 1492-1503.
- [6] E. Tsouko, J. Wang, D. E. Frigo, E. Aydogdu, C. Williams, *Carcinogenesis* **2015**, *36*(9), 1051-1060.
- [7] J. M. Brannan, W. Dong, L. Prudkin, C. Behrens, R. Lotan, B. N. Bekele, I. Wistuba, F. M. Johnson, *Clin Cancer Res* **2009**, *15*(13), 4423-4430.
- [8] H. Koch, M. E. Busto, K. Kramer, G. Medard, B. Kuster, *J Proteome Res* **2015**, *14*(6), 2617-2625.
- [9] P. D. Dunne, S. Dasgupta, J. K. Blayney, D. G. McArt, K. L. Redmond, J. A. Weir, C. A. Bradley, T. Sasazuki, S. Shirasawa, T. Wang, S. Srivastava, C. W. Ong, K. Arthur, M. Salto-Tellez, R. H. Wilson, P. G. Johnston, S. Van Schaeybroeck, *Clin Cancer Res* **2015**, *22*(1), 230-242.
- [10] C. Boshoff, *Nat Med* **2012**, *18*(6), 861-863.
- [11] C. C. Colpitts, J. Lupberger, C. Doerig, T. F. Baumert, *Biochim Biophys Acta* **2015**, *1854*(10 Pt B), 1657-1662.
- [12] P. Subbarayal, K. Karunakaran, A. C. Winkler, M. Rother, E. Gonzalez, T. F. Meyer, T. Rudel, *PLoS Pathog* **2015**, *11*(4), e1004846.
- [13] M. Khounlotham, S. Subbian, R. Smith, 3rd, S. L. Cirillo, J. D. Cirillo, *J Infect Dis* **2009**, *199*(12), 1797-1806.
- [14] A. Kaushansky, A. N. Douglass, N. Arang, V. Vigdorovich, N. Dambrauskas, H. S. Kain, L. S. Austin, D. N. Sather, S. H. Kappe, *Science* **2015**, *350*(6264), 1089-1092.
- [15] M. Tandon, S. V. Vemula, S. K. Mittal, *Expert Opin Ther Targets* **2011**, *15*(1), 31-51.
- [16] S. Chakraborty, M. V. Veetil, V. Bottero, B. Chandran, *Proc Natl Acad Sci U S A* **2012**, *109*(19), E1163-1172.
- [17] R. Noberini, I. Lamberto, E. B. Pasquale, *Semin Cell Dev Biol* **2012**, *23*(1), 51-57.
- [18] C. J. Lim, K. S. Oh, J. D. Ha, J. H. Lee, H. W. Seo, C. H. Chae, D. G. Kim, M. J. Lee, B. H. Lee, *Bioorg Med Chem Lett* **2014**, *24*(17), 4080-4083.
- [19] Q. Chang, C. Jorgensen, T. Pawson, D. W. Hedley, *Br J Cancer* **2008**, *99*(7), 1074-1082.
- [20] S. Heinzlmeir, D. Kudlinzki, S. Sreeramulu, S. Klaeger, S. L. Gande, V. Linhard, M. Wilhelm, H. Qiao, D. Helm, B. Ruprecht, K. Saxena, G. Medard, H. Schwalbe, B. Kuster, *ACS Chem Biol* **2016**, *11*(12), 3400-3411.
- [21] M. Bantscheff, D. Eberhard, Y. Abraham, S. Bastuck, M. Boesche, S. Hobson, T. Mathieson, J. Perrin, M. Raida, C. Rau, V. Reader, G. Sweetman, A. Bauer, T. Bouwmeester, C. Hopf, U. Kruse, G. Neubauer, N. Ramsden, J. Rick, B. Kuster, G. Drewes, *Nat Biotechnol* **2007**, *25*(9), 1035-1044.
- [22] G. Medard, F. Pachi, B. Ruprecht, S. Klaeger, S. Heinzlmeir, D. Helm, H. Qiao, X. Ku, M. Wilhelm, T. Kuehne, Z. Wu, A. Dittmann, C. Hopf, K. Kramer, B. Kuster, *J Proteome Res* **2015**, *14*(3), 1574-1586.
- [23] S. Klaeger, B. Gohlke, J. Perrin, V. Gupta, S. Heinzlmeir, D. Helm, H. Qiao, G. Bergamini, H. Handa, M. M. Savitski, M. Bantscheff, G. Medard, R. Preissner, B. Kuster, *ACS Chem Biol* **2016**, *11*(5), 1245-1254.
- [24] P. Bamborough, D. Drewry, G. Harper, G. K. Smith, K. Schneider, *J Med Chem* **2008**, *51*(24), 7898-7914.
- [25] M. I. Davis, J. P. Hunt, S. Herrgard, P. Ciceri, L. M. Wodicka, G. Pallares, M. Hocker, D. K. Treiber, P. P. Zarrinkar, *Nat Biotechnol* **2011**, *29*(11), 1046-1051.

- [26] C. Bardelle, B. Barlaam, N. Brooks, T. Coleman, D. Cross, R. Ducray, I. Green, C. L. Brempt, A. Olivier, J. Read, *Bioorg Med Chem Lett* **2010**, 20(21), 6242-6245.
- [27] J. Das, P. Chen, D. Norris, R. Padmanabha, J. Lin, R. V. Moquin, Z. Shen, L. S. Cook, A. M. Doweiko, S. Pitt, S. Pang, D. R. Shen, Q. Fang, H. F. de Fex, K. W. McIntyre, D. J. Shuster, K. M. Gillooly, K. Behnia, G. L. Schieven, J. Wityak, J. C. Barrish, *J Med Chem* **2006**, 49(23), 6819-6832.
- [28] A. Novak, L. D. Humphreys, M. D. Walker, S. Woodward, *Tetrahedron Lett* **2006**, 47(32), 5767-5769.
- [29] D. Glynn, D. Bernier, S. Woodward, *Tetrahedron Lett* **2008**, 49(39), 5687-5688.
- [30] A. F. Rudolf, T. Skovgard, S. Knapp, L. J. Jensen, J. Berthelsen, *PLoS One* **2014**, 9(6), e98800.
- [31] M. W. Karaman, S. Herrgard, D. K. Treiber, P. Gallant, C. E. Atteridge, B. T. Campbell, K. W. Chan, P. Ciceri, M. I. Davis, P. T. Edeen, R. Faraoni, M. Floyd, J. P. Hunt, D. J. Lockhart, Z. V. Milanov, M. J. Morrison, G. Pallares, H. K. Patel, S. Pritchard, L. M. Wodicka, P. P. Zarrinkar, *Nat Biotechnol* **2008**, 26(1), 127-132.
- [32] P. P. Graczyk, *J Med Chem* **2007**, 50(23), 5773-5779.
- [33] J. C. Uitdehaag, G. J. Zaman, *BMC Bioinformatics* **2011**, 12, 94.
- [34] S. L. Gande, K. Saxena, S. Sreeramulu, V. Linhard, D. Kudlinzki, S. Heinzlmeir, A. J. Reichert, A. Skerra, B. Kuster, H. Schwalbe, *Chembiochem* **2016**, 1439-7633.
- [35] P. Zhou, J. Zou, F. Tian, Z. Shang, *J Chem Inf Model* **2009**, 49(10), 2344-2355.
- [36] A. Moghaddas Gholami, H. Hahne, Z. Wu, F. J. Auer, C. Meng, M. Wilhelm, B. Kuster, *Cell Rep* **2013**, 4(3), 609-620.
- [37] H. Miao, D. Q. Li, A. Mukherjee, H. Guo, A. Petty, J. Cutter, J. P. Basilion, J. Sedor, J. Wu, D. Danielpour, A. E. Sloan, M. L. Cohen, B. Wang, *Cancer Cell* **2009**, 16(1), 9-20.
- [38] J. Cox, M. Mann, *Nat Biotechnol* **2008**, 26(12), 1367-1372.
- [39] J. Cox, N. Neuhauser, A. Michalski, R. A. Scheltema, J. V. Olsen, M. Mann, *J Proteome Res* **2011**, 10(4), 1794-1805.
- [40] J. Cox, M. Y. Hein, C. A. Luber, I. Paron, N. Nagaraj, M. Mann, *Mol Cell Proteomics* **2014**, 13(9), 2513-2526.
- [41] C. Ritz, J. C. Streibig, *J. Statist. Software* **2005**, 12(5).
- [42] S. Tyanova, T. Temu, P. Sinitcyn, A. Carlson, M. Y. Hein, T. Geiger, M. Mann, J. Cox, *Nat Methods* **2016**, 13(9), 731-740.
- [43] T. Anastassiadis, S. W. Deacon, K. Devarajan, H. Ma, J. R. Peterson, *Nat Biotechnol* **2011**, 29(11), 1039-1045.
- [44] U. Mueller, R. Förster, M. Hellmig, F. U. Huschmann, A. Kastner, P. Malecki, S. Pühringer, M. Röwer, K. Sparta, M. Steffien, M. Uhlein, P. Wilk, M. C. Weiss, *Eur. Phys. J. Plus* **2015**, 130, 141-150.
- [45] M. Cianci, G. Bourenkov, G. Pompidor, I. Karpics, J. Kallio, I. Bento, M. Roessler, F. Cipriani, S. Fiedler, T. R. Schneider, *J Synchrotron Radiat* **2017**, 24(Pt 1), 323-332.
- [46] M. Krug, M. Weiss, U. Heinemann, U. Mueller, *J. Appl. Cryst.* **2012**(45), 568-572.
- [47] A. J. McCoy, R. W. Grosse-Kunstleve, P. D. Adams, M. D. Winn, L. C. Storoni, R. J. Read, *J Appl Crystallogr* **2007**, 40(Pt 4), 658-674.
- [48] P. Emsley, K. Cowtan, *Acta Crystallogr D Biol Crystallogr* **2004**, 60(Pt 12 Pt 1), 2126-2132.
- [49] P. V. Afonine, R. W. Grosse-Kunstleve, N. Echols, J. J. Headd, N. W. Moriarty, M. Mustyakimov, T. C. Terwilliger, A. Urzhumtsev, P. H. Zwart, P. D. Adams, *Acta Crystallogr D Biol Crystallogr* **2012**, 68(Pt 4), 352-367.
- [50] R. A. Laskowski, M. B. Swindells, *J Chem Inf Model* **2011**, 51(10), 2778-2786.
- [51] J. A. Vizcaino, R. G. Cote, A. Csordas, J. A. Dienes, A. Fabregat, J. M. Foster, J. Griss, E. Alpi, M. Birim, J. Contell, G. O'Kelly, A. Schoenegger, D. Ovelheiro, Y. Perez-Riverol, F. Reisinger, D. Rios, R. Wang, H. Hermjakob, *Nucleic Acids Res* **2013**, 41(Database issue), D1063-1069.

Legends for figures and schemes

Figure 1. EPHA2 inhibitor design by hybridization of known EPH receptor binders. a) The dual BCR-ABL/SRC inhibitor Dasatinib comprises a very broad selectivity profile targeting 44 proteins with sub-micromolar affinities across several kinase families. Dasatinib is the most potent known EPHA2 inhibitor and was chosen as molecular scaffold for the development of dedicated EPHA2 inhibitors. b) Hybridization of known EPH binders (Dasatinib, EPHB4 inhibitors, CHEMBL249097, PD-173955) motivated the introduction of morpholino and methylsulfonyl moieties, the substitution of Dasatinib's pyrimidine by an aryl moiety, and the introduction of an amide bond in *meta*-position. c) Inhibitor design comprised a *N*-(2-chloro-6-methylphenyl)-2-(arylamino)thiazole-5-carboxamide scaffold binding the nucleotide binding pocket and chemical modifications which were introduced at positions R' and R'' to engage interactions within the ribose pocket and/or the ATP pocket entrance, respectively.

Figure 2. Synthesis scheme for EPHA2 inhibitors. a) Compound I, *n*-butyllithium, THF, -78°C , 15 min, argon; 2-chloro-6-methylphenyl isocyanate, THF, -78°C , 2h, argon (70-80% yield). b) Compound II, ethyl 3-aminobenzoate, (+)-camphor-10-sulfonic acid, 2-propanol, MW, 120°C , 3h, argon (66-76% yield). c) DABAL-Me₃, primary amine, THF, 40°C , 30 min; Compound III, THF, MW, $100-140^{\circ}\text{C}$, 2-6 h (3-91 % yields). d) Compound II, (+)-camphor-10-sulfonic acid, 5-substituted 3-aminobenzoic acids, *tert*-butanol, MW, 120°C , 3.5 h (28-92% yield). e) Compound V, primary amine, DMF, 0°C ; DIEA, TEA, PyBroP, DMF, 30-140 min (4-74% yield). f) Compound V, tributyl(vinyl)tin, dioxane, toluene, Pd(PPh₃)₄, 110°C , 4h, argon (59% yield). g) Inhibitor 3a, 2-aminobenzenboronic acid, Pd(PPh₃)₄, DMF; K₂CO₃, MW, 115°C , 5h, argon (32% yield). h) 3,5-substituted aniline, 2-propanol, compound II, HCl, ON, 95°C (26-43%).

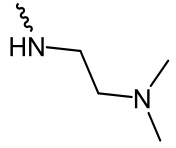
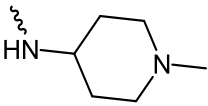
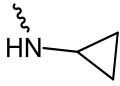
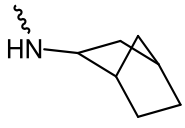
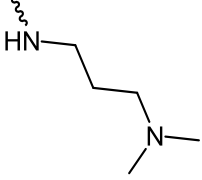
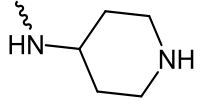
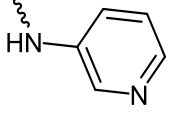
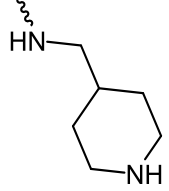
Figure 3. Selectivity profiles of EPHA2 inhibitors. a) Heatmap showing selectivity profiles and apparent binding affinities (pK_d^{app} [M]) of Dasatinib and EPHA2 inhibitor candidates. Target kinases are sorted according to kinase phylogeny. EPHA2 is highlighted by a black box. b) Selectivity of EPHA2 inhibitors as obtained by simple target counting (upper panel) or the EPHA2-specific CATDS_{EPHA2} score (concentration and target dependent selectivity, lower panel). Inhibitor **4a** was found to be the most potent and most selective EPHA2 inhibitor in our panel. c) Radar plots depicting the target space and binding affinities of

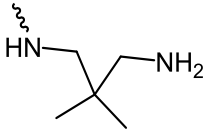
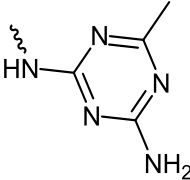
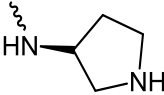
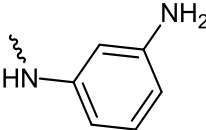
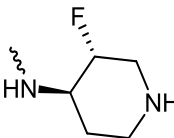
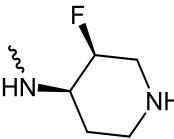

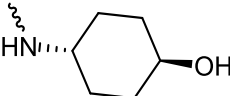
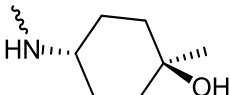
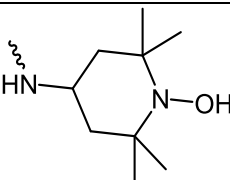
inhibitor **2g** which showed the lowest number of targets but also lowest affinity for EPHA2 (upper panel), and inhibitor **4a** that has the highest affinity and selectivity for EPHA2 (lower panel).

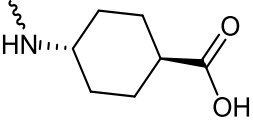
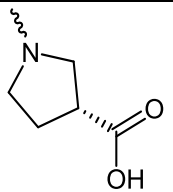
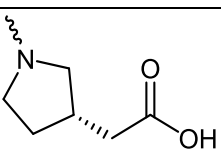
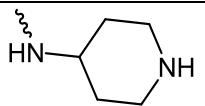
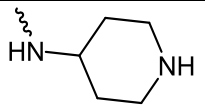
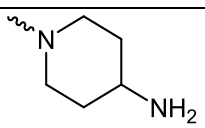

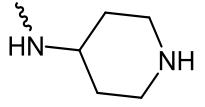
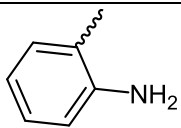
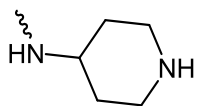
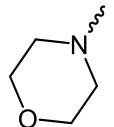
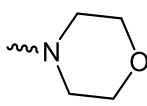
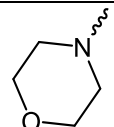
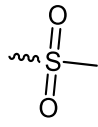
Figure 4. Inhibitor-EPHA2 co-crystal structures validate medicinal chemistry concept. a) All 17 EPHA2 inhibitor candidates bound in the type 1 conformation (DFG-in) in the ATP binding site located between the N lobe and the C lobe. b) The inhibitors engaged both, the ATP pocket entrance and the ribose pocket. c) In most inhibitors, the introduced amide bond formed direct side chain interactions with Tyr694 and Glu696 located towards the ATP pocket entrance. In some inhibitors, another conformation involving backbone interactions to Ile619 and Ala699 in the ribose pocket was observed. d) As intended, selectivity residues Lys617, Lys702, Glu706 were often engaged in direct or water-mediated interactions by inhibitors carrying an amine, hydroxyl or carboxyl group. Surprisingly, inhibitor **2g** carrying a carboxylic moiety adapted an unexpected bent conformation and interacted with Tyr694 (indicated by dashed line).

Figure 5. Inhibitor 4a shows anti-proliferative effects in the SF-268 glioblastoma cell line. a) Kinome profiling of the NCI60 panel of cancer cell lines revealed that SF-268 cells feature high EPHA2 expression and low abundance of other targets (bar chart) frequently hit by our EPHA2 inhibitors (bar color). Inhibitor targets were sorted according to the maximum observed affinity (pK_d^{app} [M]) within our dataset and theoretical therapeutic windows were set at 10x and 100x K_d^{app} of EPHA2. b) Protein knockdown of EPHA2 by four independent siRNAs confirmed that SF-268 cell viability is dependent on EPHA2 expression. Experiments were performed in three biological replicates each containing three technical replicates. Significance was calculated by a two-sided unpaired student's t-test. c) SF-268 cells were treated with increasing concentrations of inhibitor **4a** resulting in potent reduction of cell viability similar to Dasatinib.

Table 1. Synthesis and affinity of EPHA2 inhibitors. Chemical modifications were introduced at R' and R'' according to synthesis methods A, B or C. Binding inhibition was determined in single dose Kinobeads pulldowns.

Inhibitor	R'	R''	Method	Yield [%]	% Binding Inhibition
Dasatinib	-	-	-	-	100 ^[a]
1a	H	methyl	A	28	75 ^[b]
1b	H		A	85	68 ^[b]
1c	H		A	16	74 ^[b]
1d	H		A	63	57 ^[b]
1e	H		A	91	< 50 ^[b]
1f	H		A	78	< 50 ^[b]
1g	H		A	44	95 ^[b]
1h	H		A	23	< 50 ^[b]
1i	H		A	52	< 50 ^[b]

1j	H		A	21	83 ^[b]
1k	H		A	3	64 ^[b]
1l	H		A	17	94 ^[b]
1m	H		A	48	59 ^[b]
2a	H		B	63	50 ^[a]
2b	H		B	quant	64 ^[a]
2c	H		B	4	95 ^[a]
2d	H		B	74	56 ^[a]
2e	H		B	54	43 ^[a]
2f	H		B	29	67 ^[a]

2g	H		B	50	40 ^[a]
2h	H		B	55	93 ^[a]
2i	H		B	72	93 ^[a]
3a	Br		B	60	89 ^[b]
3b	CF ₃		B	67	88 ^[b]
3c	Br		B	22	53 ^[b]
3d			B	27	97 ^[b]
3e			B	32	96 ^[b]
4a			C	26	98 ^[a]
4b			C	34	95 ^[a]

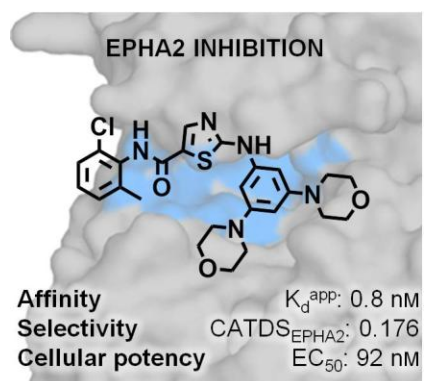
[a] as determined by quantitative mass spectrometry at 3 μ M, [b] as determined by quantitative Western Blot analysis at 10 μ M.

Table 2. Properties of EPHA2 inhibitor candidates. Promising inhibitors were further characterized according to their binding affinity, inhibition of enzymatic activity, inhibition of cell viability, and their selectivity as described by the number of sub-micromolar targets and CATDS_{EPHA2}. Crystallography data was obtained for 17 inhibitors in high resolution.

Inhibitor	Affinity pK _d ^{app} [M]	Activity pIC50 [M]	Cellular EC ₅₀ ± SD ^[a] [μM]	# targets < 1 μM	Selectivity CATDS _{EPHA2}	PDB code	X-ray resolution [Å]
Dasatinib	8.23	-	0.097 ± 0.020	44	0.047	5I9Y	1.23
1c	-	-	2.67 ± 0.53	-	-	-	-
1g	7.78	-	4.41 ± 2.69	22	0.074	5NJZ	1.77
1j	-	-	-	-	-	5NK0	1.60
1k	-	-	-	-	-	5NK1	1.55
1l	7.42	-	-	26	0.057	5NK3	1.82
1m	-	-	-	-	-	5NK5	1.35
2a	6.33	-	1.99 ± 0.24	21	0.032	5NK7	1.89
2b	6.74	-	1.54 ± 0.79	23	0.033	-	-
2c	8.70	9.00	1.40 ± 0.13	26	0.141	5NK4	1.45
2d	6.80	-	2.38 ± 0.75	20	0.051	5NK6	1.27
2e	6.14	-	2.32 ± 0.30	16	0.037	5NK9	1.59
2f	6.64	8.52	3.10 ± 0.94	16	0.057	5NK8	1.76
2g	5.46	-	> 5	13	0.026	5NKA	1.38
2h	7.73	-	> 5	17	0.063	-	-
2i	7.58	7.74	> 5	23	0.066	-	-
3a	-	-	-	-	-	5NKE	1.39
3c	-	-	-	-	-	5NKF	1.10
3d	7.68	-	-	28	0.066	5NKG	1.10
3e	7.59	-	-	22	0.056	5NKH	1.29
4a	9.12	-	0.092 ± 0.021	31	0.176	5NKB	1.50
4b	7.73	8.47	0.506 ± 0.034	26	0.050	5NKI	1.68

[a] Cellular EC₅₀ values represent the mean \pm SD of three independent biological replicates each performed in three technical replicates.

Table of content



Chemoproteomics-guided drug discovery: Chemical proteomics was used to guide a drug discovery program towards novel inhibitors targeting the receptor tyrosine kinase EPHA2. We discovered compound 4a as a valuable inhibitor with low nanomolar affinity, an improved selectivity profile and promising anti-proliferative effects.